Current Sensorless Control for Bidirectional Full-Bridge Converter in DC Distributed System

Hung-Chi Chen and Jhen-Yu Liao
Department of Electrical and Computer Engineering, National Chiao Tung University , Hsinchu, Taiwan

***Abstract*—In this paper, the average behavior of a bidirectional AC-DC converter is analyzed and simplified to an equivalent single-switch model. Based on this single-switch model, new current sensorless control without any current loop is developed and implemented. Compared with the conventional multi-loop control, the proposed current sensorless control is able to regulate DC-side voltage and yield sinusoidal current in phase with the AC input voltage simultaneously. The provided simulation and experiment results also demonstrate the proposed current sensorless control.**

I. INTRODUCTION

Use of renewable energy is gaining more attention with increasing concern about possible energy crisis and environmental issues. The outputs of photovoltaic panel and fuel cell stack are variable dc, while the outputs of most wind generation systems are variable ac. Therefore, the renewable energy cannot be connected to the grid directly. In practice, to effectively utilize the energy generated by alternate energy sources, power converters play a key part in all renewable energy generation systems.

To incorporate different types of renewable energy generation systems into the grid system, a dc bus is commonly used as shown in Fig. 1 [1-2]. The varying dc output of photovoltaic panels and fuel cell stacks are connected with a common dc bus via dc/dc converters. Small-scale wind generators, most of which are permanent-magnet synchronous generator (PMSG) can be connected with the dc bus through ac/dc converters.

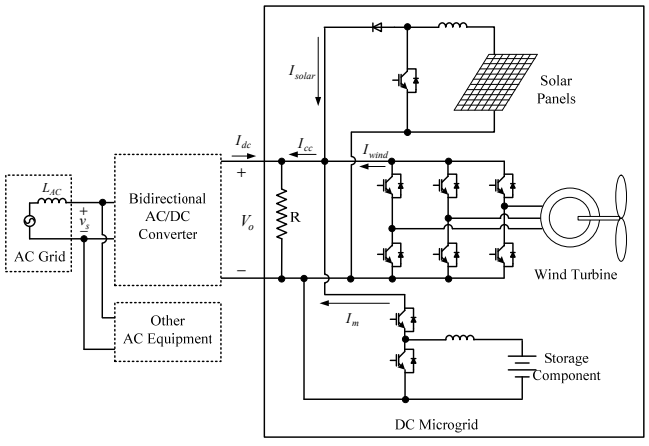

Fig. 1 Grid-tied DC microgrid with distributed renewable sources and storage components.

The dc bus voltage is kept nearly a constant and can be interfaced with the commercial AC grid by means of DC/AC converters. The commonly used DC/AC grid-connected converter is the PWM voltage source inverter (VSI) [2-4] that requires a dc link front-end with voltage level higher than the peak value of grid voltage. In such systems, line frequency transformer has to be used when electrical isolation is required between the dc bus and the utility line.

Bi-direction AC/DC converter links the DC and AC sides and therefore, it is essential for renewable energy system and DC distributed system. Four-switch full-bridge converter is often used in single-phase system. The study of inverter operation and rectifier operation can be found in [5-6] and [7-8], respectively. Conventional multiloop control with inner current loop and outer voltage loop can also be used in [9].

Sensorless control has been developed in the boost converter. Sensorless control reduces the number of the sensor and use some algorithms to achieve the PFC function. It can be classified to voltage sensorless control and current sensorless control. Voltage sensorless control can inherently provide electrical isolation between the power circuit and the controller [10]. However, the current sampling rate must as high as the switching frequency. On the other hand, current sensorless control has advantage of not been affected by the switching noise [11]. Current command of current sensorless control also not been affected by the output voltage ripple. However, no current sensorless control had ever been used in the bi-directional converter. In this paper, the current sensorless control for bi-directional converter is well developed and demonstrated.

The paper is organized as follows. Initially, the behavior of a bidirectional full-bridge converter is studied and the equivalent single-switch model is also derived. Based on this model, the current sensorless control is proposed and the yielded current is in phase with the input voltage. Finally, some simulated and experimental results have been given to illustrate the bidirectional performances of the proposed control.

II. Modeling of Bidirectional AC/DC Converter

Fig. 1 shows the bidirectional AC/DC converter and the dc-side current and the net dc-side current are denoted as I_{dc} and I_{cc}, respectively. When equivalent current I_{dc} is positive, some energy should be moved to the dc side in order to keep the dc-side voltage and thus, the converter

needs to operate in rectifier mode. Contrary, when current I_{dc} is negative, excess energy should be removed from dc side and thus, the converter needs to operate at inverter mode.

Fig. 2 shows the used full-bridge converter topology and the dc side current is represented as a current source I_{dc}. The four switching signals are generated according to the three inputs $sign(I_{dc})$, $sign(v_s)$ and the switching signal $d(t)$ where the PWM signal $d(t)$ is generated from the proposed current sensorless control and

$$sign(x) = \begin{cases} 1, \text{when } x \geq 0 \\ 0, \text{when } x < 0 \end{cases} \quad (1)$$

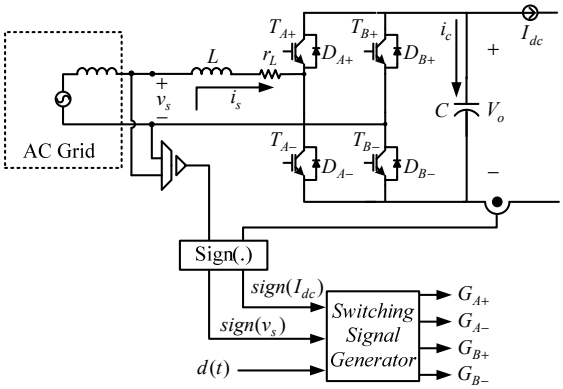

Fig. 2 Bidirectional AC-DC converter with switching signal generation.

According to the unique switching signal $d(t)$, the sign value $sign(v_s)$ of input voltage v_s and the power direction signal $sign(I_{dc})$, four switching signals G_{A+}, G_{A-}, G_{B+} and G_{B-} are generated based on the following rules as tabulated in Table I.

$$G_{A+} = \overline{sign(I_{dc})} \cdot sign(v_s) + sign(I_{dc}) \cdot \overline{sign(v_s)} \cdot d(t) \quad (2)$$

$$G_{A-} = \overline{sign(I_{dc})} \cdot \overline{sign(v_s)} + sign(I_{dc}) \cdot sign(v_s) \cdot d(t) \quad (3)$$

$$G_{B+} = \overline{sign(I_{dc})} \cdot \overline{sign(v_s)} \cdot \overline{d(t)} \quad (4)$$

$$G_{B-} = \overline{sign(I_{dc})} \cdot sign(v_s) \cdot \overline{d(t)} \quad (5)$$

It is also noted that after analysis, the power direction signal $sign(I_{dc})$ can be equivalently replaced by the sign value $sign(\hat{V}_L)$ of the control signal $\hat{V}_L$. Therefore, the proposed control does not sense any current.

From the power direction of bidirectional AC/DC converter, the operation can be divided into rectifier mode and inverter mode. In rectifier mode, the direction of power flow is from AC-side to DC-side. In order to obtain the single-switch mode, the average behaviors in rectifier mode and inverter mode are analyzed, respectively.

A. Rectifier Operation ($sign(I_{dc}) = 1$)

According to (2)-(5), the gate signals during the positive input voltage ($sign(v_s) = 1$) and during the negative input voltage ($sign(v_s) = 0$) can be summarized as (6) and (7), respectively.

$$G_{A+} = 0, \; G_{A-} = d(t), \; G_{B+} = 0, \; G_{B-} = 0, \quad (6)$$

$$G_{A+} = d(t), \; G_{A-} = 0 \; G_{B+} = 0, \; G_{B-} = 0, \quad (7)$$

Since the switching signal $d(t)$ is either $d(t)$ =1 or $d(t)$ =0, the resulting current flowing paths during positive input voltage and negative input voltage are plotted in Fig. 3 and Fig. 4, respectively. From the case of $d(t)$ =1 in Fig. 3(a) and Fig. 4(a), the equivalent KVL equation regardless of the input voltage polarity $sign(v_s)$ can be expressed as

$$v_L = v_s - [2sign(v_s) - 1]V_F - r_L i_s \quad (8)$$

where V_F represents the sum of conduction voltages of semiconductor switches.

From the circuit of $d(t)$ =0 as shown in Fig. 3(b) and Fig. 4(b), the equivalent KVL equation can also be obtained by the equation

$$v_L = v_s - [2sign(v_s) - 1]V_F - r_L i_s - [2sign(v_s) - 1]V_o \quad (9)$$

Table I Summary of Switching Signal

$sign(I_{dc})$	$sign(v_s)$	$d(t)$	G_{A+}	G_{A-}	G_{B+}	G_{B-}	Conducting path	V_{AB}
1	1	1	0	1	0	0	$G_{A-} + D_{B-}$	0
		0		0			$D_{A+} + D_{B-}$	V_o
	0	1	1	0	0	0	$D_{A+} + D_{B+}$	0
		0	0				$D_{A-} + D_{B+}$	$-V_o$
0	1	1	1	0	0	0	$T_{A+} + D_{B+}$	0
		0				1	$T_{A+} + T_{B-}$	V_o
	0	1	0	1	0	0	$T_{A-} + D_{B-}$	0
		0			1		$T_{A-} + T_{B+}$	$-V_o$

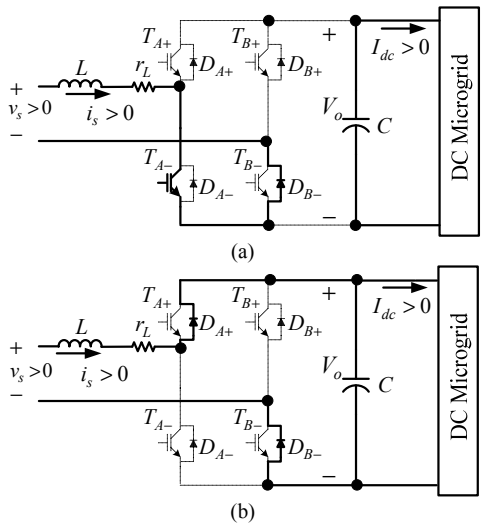

Fig. 3 Conducting path with rectifier operation $sign(I_{dc})=1$, positive input voltage $sign(v_s)=1$ and switching signal (a) $d(t)=1$, (b) $d(t)=0$.

B. Inverter Operation ($sign(I_{dc})=0$)

Similarly, the gate signals during the positive input voltage ($sign(v_s)=1$) and during the negative input voltage ($sign(v_s)=0$) can be summarized as (10) and (11), respectively.

$$G_{A+}=1,\ G_{A-}=0,\ G_{B+}=0,\ G_{B-}=\overline{d(t)}, \tag{10}$$

$$G_{A+}=0,\ G_{A-}=1\ G_{B+}=\overline{d(t)},\ G_{B-}=0, \tag{11}$$

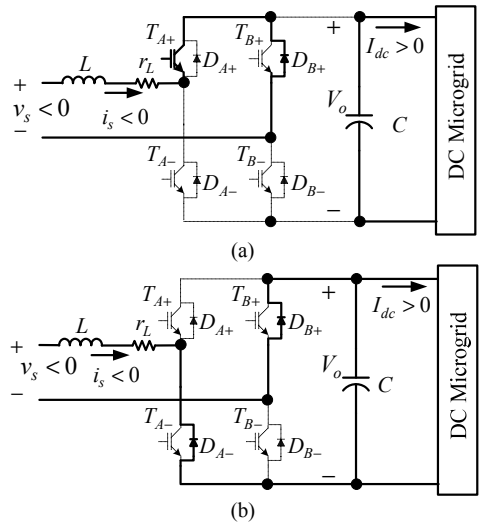

Fig. 4 Conducting path with rectifier operation $sign(I_{dc})=1$, positive input voltage $sign(v_s)=0$ and switching signal (a) $d(t)=1$, (b) $d(t)=0$.

In addition, the resulting current flowing paths during positive input voltage and negative input voltage are plotted in Fig. 5 and Fig.6, respectively. From Fig. 5(a) and Fig. 6(a), their KVL equations for $d(t)$ =1 regardless of the input voltage polarity $sign(v_s)$ can be combined to the equation

$$v_L = v_s + [2sign(v_s)-1]V_F - r_L i_s \tag{12}$$

From Fig. 5(b) and Fig. 6(b), the combined KVL equations for $d(t)$ =0 can be expressed as

$$v_L = v_s + [2sign(v_s)-1]V_F - r_L i_s - [2sign(v_s)-1]V_o \tag{13}$$

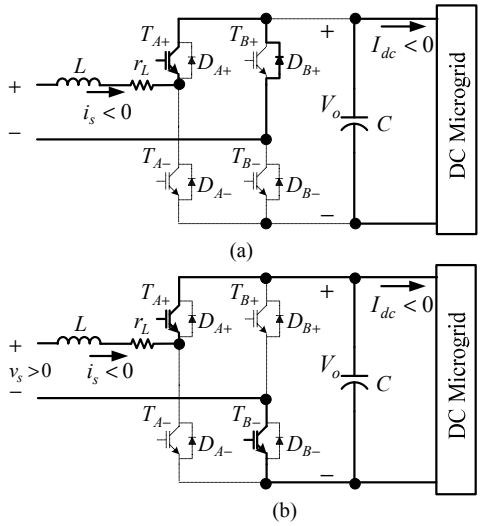

Fig. 5 Conducting path with inverter operation $sign(I_{dc})=0$, positive input voltage $sign(v_s)=1$ and switching signal (a) $d(t)=1$, (b) $d(t)=0$.

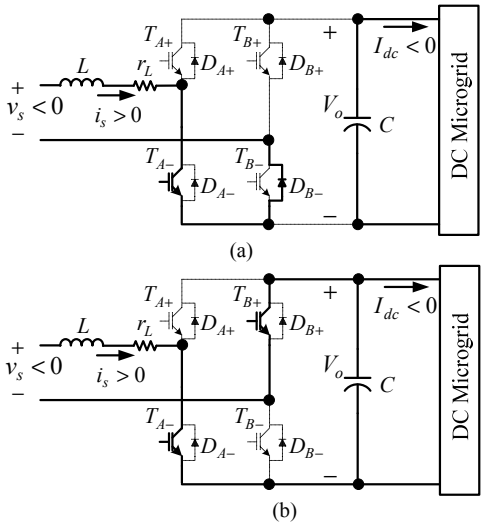

Fig. 6 Conducting path with inverter operation $sign(I_{dc})=0$, positive input voltage $sign(v_s)=0$ and switching signal (a) $d(t)=1$, (b) $d(t)=0$.

C. Single-Switch Modelling

By considering the combined equation (8) in rectifier mode and the combined equation (12) in inverter mode, the equivalent KVL equation for $d(t)$=1 regardless of power direction $sign(I_{dc})$ and input voltage polarity $sign(v_s)$ can be expressed as

$$v_L = v_s - [2sign(I_{dc})-1][2sign(v_s)-1]V_F - r_L i_s \quad (14)$$

Similarly, the equivalent KVL equation for $d(t)$=0 can be expressed as

$$\begin{aligned} v_L &= v_s - [2sign(I_{dc})-1][2sign(v_s)-1]V_F \\ &\quad - r_L i_s - [2sign(v_s)-1]V_o \end{aligned} \quad (15)$$

Consequently, the average inductor voltage $\bar{v}_L$ can be obtained from multiplying (14) by the average conducting time $\bar{d}T_s$ and multiplying (15) by the average blocking time $(1-\bar{d})T_s$. Therefore, the single-switch model for bidirectional AC/DC converter has been derived and can be plotted in Fig. 7.

$$\begin{aligned} \bar{v}_L &= v_s - [2sign(I_{dc})-1][2sign(v_s)-1]V_F \\ &\quad - r_L i_s - (1-\bar{d})\cdot[2sign(v_s)-1]V_o \end{aligned} \quad (16)$$

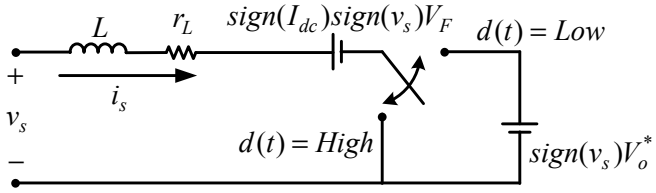

Fig. 7 Equivalent single-switch modeling of full-bridge AC/DC converter in Fig. 2.

III. Proposed Current Sensorless Control

The proposed current sensorless control is plotted in Fig. 8 where the switching signal $d(t)$ is obtained from the comparison result of control signal v_{cont} and unit triangular signal v_{tri} varying between 0 to 1. Thus, the average value $\bar{d}$ of switching signal can be expressed as $\bar{d} = 1 - v_{cont}$.

In order to yield sinusoidal input current $i_s = \hat{I}_s \sin(\omega t)$ in phase with the input voltage $v_s = \hat{V}_s \sin(\omega t)$, the average inductor voltage $\bar{v}_L$ in (16) must be the function of $\cos(\omega t)$. Therefore, the desired average inductor voltage can be expressed as $\bar{v}_L = \hat{V}_L \cos(\omega t)$ where $\hat{V}_L$ is the inductor voltage amplitude. By substituting $\bar{v}_L = \hat{V}_L \cos(\omega t)$ into (16), the control signal v_{cont} must be

$$v_{cont} = (1-\bar{d}) = \frac{1}{V_o^*}[|v_s| - sign(I_{dc})V_F - \hat{V}_L(s_1 + s_2 \frac{r_L}{\omega L})] \quad (17)$$

where $s_1 = sign(v_s)\cdot\cos(\omega t)$ and $s_2 = |\sin(\omega t)|$ are two synchronized signals generated from the input voltage v_s .

Once the inductor voltage $\bar{v}_L$ is forced to follow the function of $\cos(\omega t)$, the average input current must be $\bar{i}_s = \bar{i}_L = [\hat{V}_L/(\omega L)]\sin(\omega t)$ and the yielded average power $\bar{P}$ become

$$\bar{P} = \hat{V}_s \hat{V}_L / (2\omega L) \quad (18)$$

where the inductor voltage amplitude $\hat{V}_L$ is a bipolar signal, and thus, the average power $\bar{P}$ is proportional to the amplitude $\hat{V}_L$.

Equation (18) is very important for the proposed current sensorless control. First, the amplitude $\hat{V}_L$ can be easily obtained by introducing a PI-type voltage controller in the proposed current sensorless control to regulate the DC-side voltage V_o based on the balance between the input power $\bar{P} = \hat{V}_s \hat{V}_L / (2\omega L)$ and DC-side net power $V_o I_{dc}$. Therefore, the amplitude $\hat{V}_L$ is not obtained by any calculation.

Additionally, it can be found that from (18), the average power $\bar{P}$ is positive when the sign value $sign(\hat{V}_L)$ is also positive and thus, the converter operates in the rectifier mode. One the other hand, the average power $\bar{P}$ is negative when the sign value $sign(\hat{V}_L)$ is also negative and thus, the converter operates in the inverter mode. It implies that the sign value $sign(\hat{V}_L)$ can be used to replace for the sign value $sign(I_{dc})$ in Fig. 1 and (17) without sensing net current I_{dc} . Thus, the resulting control signal can be obtained by

$$v_{cont} = \frac{1}{V_o^*}[|v_s| - sign(\hat{V}_L)V_F - \hat{V}_L(s_1 + s_2 \frac{r_L}{\omega L})] \quad (19)$$

In Fig. 8, the control signal v_{cont} is obtained according to (19).

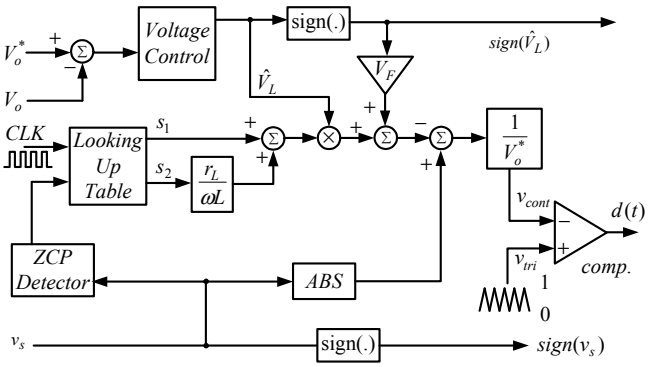

Fig. 8 The proposed current sensorless control.

IV. Simulation Results

In this section, a series of computer simulations are performed to demonstrate the proposed current sensorless control. Some nominal values and circuit parameters are listed in Table II. The simple PI-type loop with anti-windup mechanism is used as the voltage controller in the developed current sensorless control to automatically adjust the inductor voltage amplitude $\hat{V}_L$.

Table II Simulation parameters

DC-Microgrid Voltage	$V_o^* = 200V$
DC-side Resistance	$R = 100\Omega$
Input frequency	$f = 60Hz$
Inductance	$L = 4.6mH$
Equivalent resistance	$r_L = 0.5\Omega$
Capacitance	$C_o = 1410\mu F$
Conducting voltage	$V_F = 1.61V$.
Switching frequency	$f_{tri} = 40kHz$

In the simulation, a resistor $R = 100\Omega$ is connected to the DC-side of the AC/DC converter and a constant-current current source I_{CC} is also connected to DC-side of the AC/DC converter to simulate the unknown renewable energy. Since the DC voltage is regulated to 200V, the AC/DC converter needs to operate in the inverter mode to feedback some power from DC-side to AC-side when the current source I_{CC} is larger than I_{CC}>2A.

When current source I_{CC} is zero, the AC/DC converter needs to operate in the rectifier mode to transfer 400W from AC-side to DC-side to regulate the DC-side voltage.

The simulated waveforms when the AC/DC converter operates in inverter mode and in rectifier mode are plotted in Fig. 9(a) and Fig. 9(b), respectively. In Fig. 9(a), the constant-current current source I_{CC} is zero. To supply the connected load resistor, average input power 400W is required. The yielded input current i_s is sinusoidal in phase with the input voltage v_s and the voltage amplitude $\hat{V}_L$ is tuned to about `9.2V.

On the contrary, when the constant-current current source I_{CC} is set to 4A, the introduced renewable power is larger than the resistor dissipated power and thus, excess power needs to be removed in order to keep the DC-microgrid voltage. Therefore, in Fig. 9(b), the AC/DC converter operates in inverter mode with average input power -400W. The yielded input current is sinusoidal and the tuned voltage amplitude by PI-type voltage loop is about -7.9V.

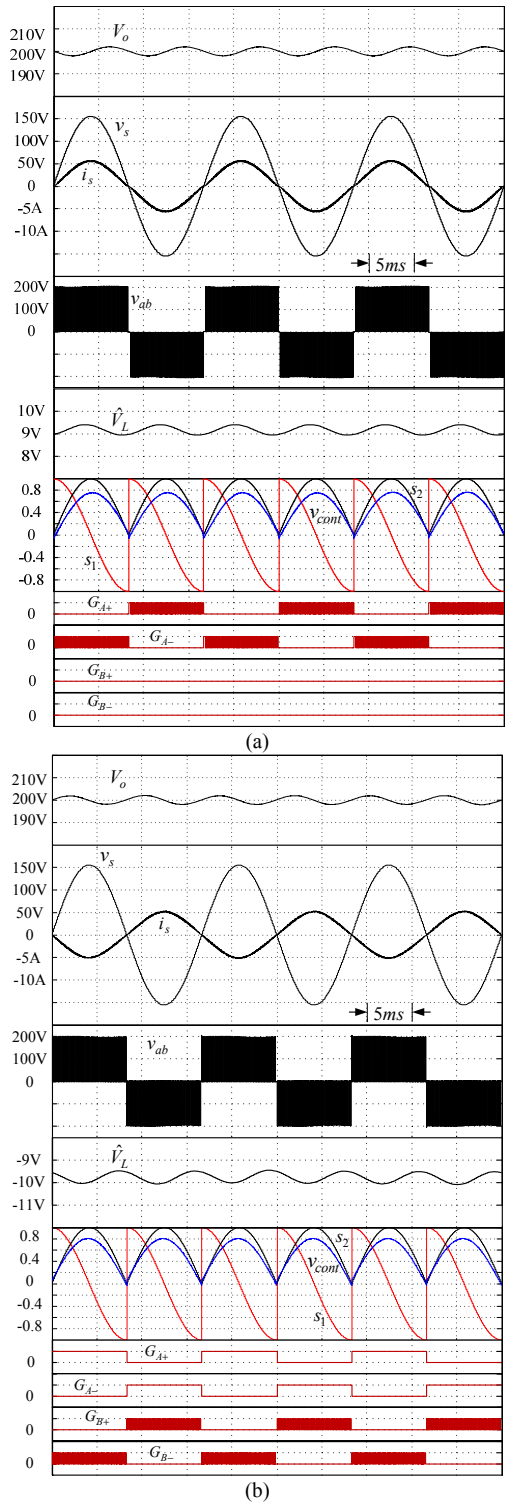

Fig. 9 Simulation results when the full-bridge converter operates (a) in rectifier mode with average input power 400W (i.e. I_{cc} =0A), (b) in inverter mode with average input power -400W (i.e. I_{cc} =4A).

In practical condition, the input voltage is often distorted due to the input inductance. To evaluate the performance of the proposed current sensorless control, the simulated waveforms with distorted voltage under inverter mode and rectifier mode are plotted in Fig. 10(a) and Fig. 10(b), respectively. Although the input voltage v_s is distorted, the yielded input currents i_s are still sinusoidal waveforms. It shows that the proposed current sensorless control is able to work well with distorted input voltage.

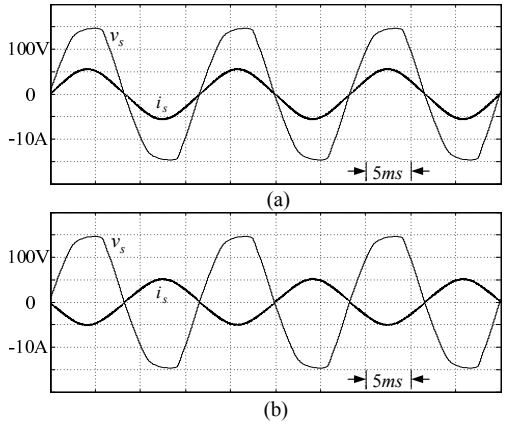

Fig. 10 Simulation results with distorted input voltage
(a) in rectifier mode with average input power 400W (i.e. I_{cc} =0A),
(b) in inverter mode with average input power -400W (i.e. I_{cc} =4A).

In order to evaluate the transient performance of the proposed current sensorless control, the simulated waveform with the sudden change of renewable energy from 0 W (I_{cc} =0A) to 800 W (I_{cc} =4A) is plotted in Fig. 11. The DC-Microgrid voltage is well regulated to 200V and the yielded input current is also sinusoidal waveforms. Due to the input inductance in the front of the full-bridge converter, the peak amplitude of the input voltage v_s also changes after the AC/DC converter operates in different mode.

All the provided simulation results demonstrate the proposed current sensorless control for AC/DC converter.

V. EXPERIMENTAL RESULTS

The experimental setup of DC-microgrid with AC/DC converter and the FPGA-based implementation of the proposed current sensorless control are plotted in Fig. 12. The circuit parameters had been tabulated in Table II. A DC source operating at constant current mode (CC mode) is connected to the DC-side to be regarded as the renewable energy.

Due to no A/D and no D/A function in commercial FPGA chip, an external A/D converter is used to sense the output voltage and a zero-crossing detecting circuit is used to detect the zero-crossing of the input voltage. Some D/A converters are used to show the control variables of the implemented current sensorless control in the scope.

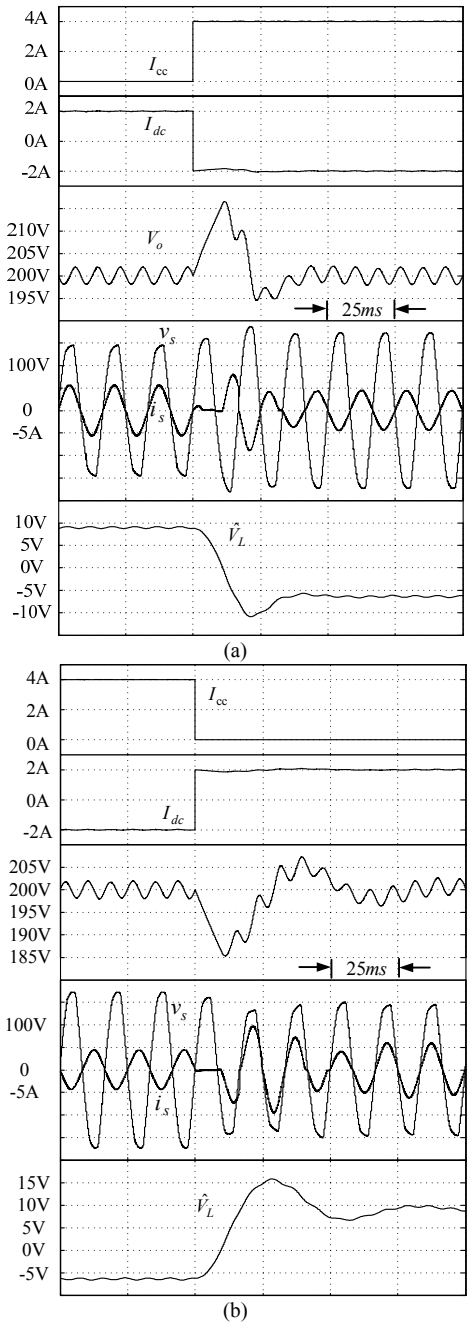

Fig. 11 Simulation results when the renewable energy suddenly changes
(a) from 0W (I_{cc} =0A) to 800W (I_{cc} =4A),
(b) from 800W (I_{cc} =4A) to 0W (I_{cc} =0A).

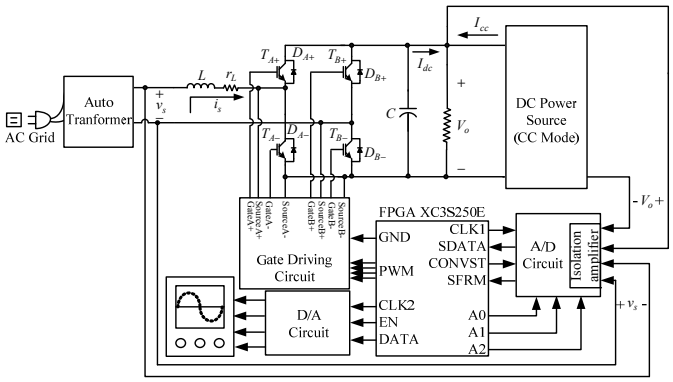

Fig.12 The experimental setup and the FPGA-based implementation of the proposed current sensorless control.

In order to provide a pure sinusoidal voltage waveform, an AC voltage source is connected to the AC-side of AC/DC converter instead of the autotransformer and AC grid in Fig. 12. The current I_{cc} in DC power source is set to zero to force the AC/DC converter operate at rectifier mode with average input power 400W. The yielded input current and voltage waveform is plotted in Fig. 13(a) where the total current harmonic distortion is about *THDi*=5.55%. Due to the difference between the nominal circuit parameter and actual parameters, the yielded current is not pure sinusoidal current waveform, but it is closed to the sinusoidal waveform.

Because that the available instrument - AC power source can not absorb power, no experimental waveform of inverter mode with sinusoidal input voltage is provided in this paper.

By plugging the AC-side of AC/DC converter into the AC-grid, the distorted input voltage is input to the AC/DC converter. The yielded input current and voltage waveforms at rectifier mode and inverter mode are plotted in Fig. 13(b) and Fig. 13(c), respectively.

In Fig. 13(b), the current I_{cc} in DC power source is set to zero and the AC/DC converter needs to operate in rectifier mode to keep the DC-Microgrid voltage. The yielded input current is in phase with the input voltage, but it is not as sinusoidal as the simulation result due to the parameter mismatch and distorted input voltage.

In Fig. 13(c), the CC-mode current I_{cc} in DC power source is set to 4A and the AC/DC converter needs to operate in inverter mode to remove excess power to regulate the DC-Microgrid voltage. The yielded input current is in phase with the input voltage, but it possesses larger current harmonics than that in Fig. 13(b).

From Fig. 14, the real current I_{cc} is not constant current source as in the simulation, but it carries some current ripple which results in larger current harmonics introduced by the proposed current sensorless control.

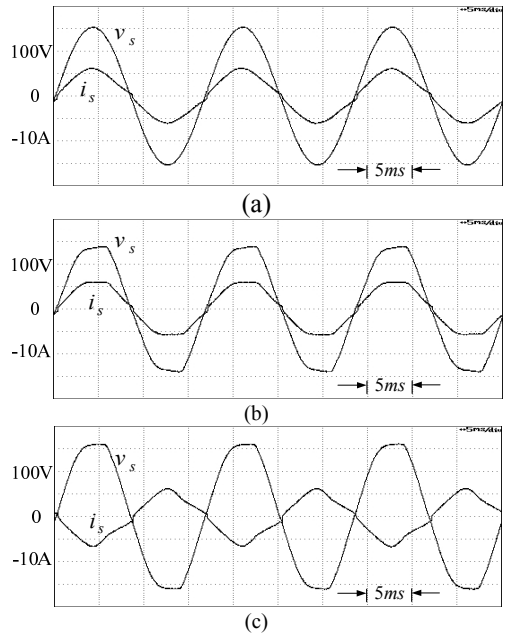

Fig. 13 Experimental waveforms
(a) with sinusoidal input voltage (rectifier operation at 400W, I_{cc} =0A);
(b) with distorted input voltage (rectifier operation at 400W, I_{cc} =0A);
(c) with distorted input voltage (inverter operation at -400W, I_{cc} =4A).

The experimental results during the change of CC-mode current I_{cc} from 0A to 4A and from 4A to 0A are plotted in Fig. 14(a) and fig. 14(b), respectively. The DC-Microgrid voltage V_o is well regulated to 200V and the yielded input current is in phase with the input voltage. Like the simulation results in Fig. 11, the amplitude of input voltage v_s may change after the AC/DC converter changes its operation mode.

Because the unknown renewable energy is synthesized by a programmable DC power source in CC mode, the significant current ripple in the current I_{cc} is resulted from the voltage ripple in DC-Microgrid voltage V_o and has a effect on the yielded input current waveform in Fig. 13(c).

In addition, the current I_{cc} cannot change suddenly like the simulations in Fig. 11 and has a significant transient time 20ms due to the available programmable DC power source. In practice, the renewable energy would not change suddenly.

Therefore, all the provided results show that the proposed current sensorless control is able to control the bidirectional AC/DC converter.

VI. CONCLUSIONS

In this paper, the single-switch model for bidirectional full-bridge converter has been developed. Based on the single-switch model, the proposed current sensorless control has been developed and implemented. The provided results show its stable operation characteristics.

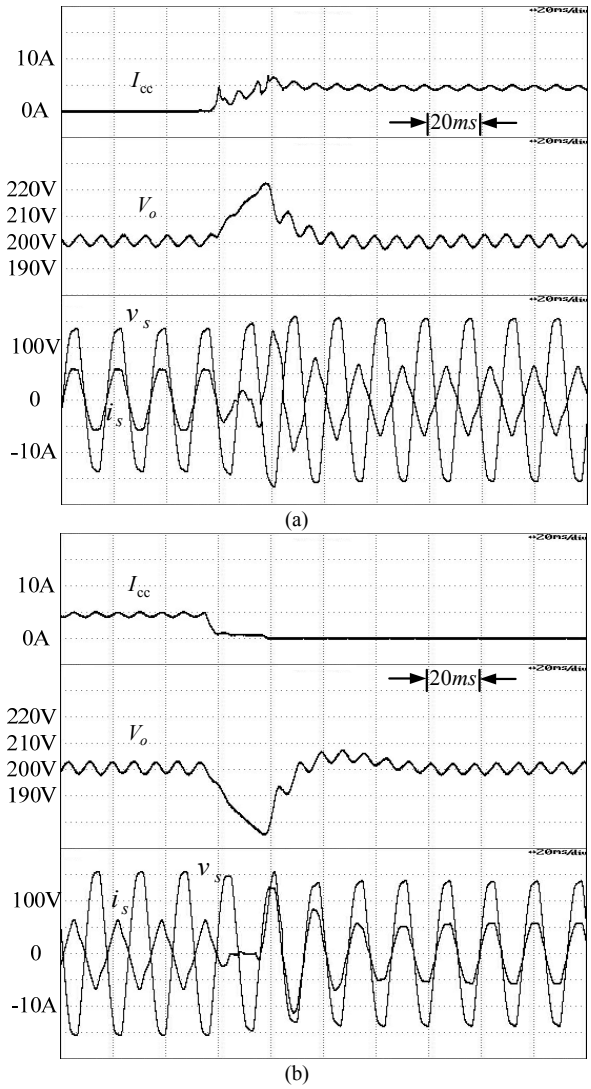

Fig. 14 Experimental waveforms during the change of the synthesized renewable energy (a) from 0W (I_{cc} =0A) to 800W (I_{cc} =4A), (b) from 800W (I_{cc} =4A) to 0W (I_{cc} =0A).

Aknowledge

This work was supported by the National Science Council of Taiwan under Contract NSC 101-3113-E-009-006.

REFERENCES

[1] B. Singh, B. N. Singh, A. Chandra, K. Al-Hadded, A. Pandey and D. P.Kothari, "A Review of Single-Phase Improved Power Quality AC/DC Converters," *IEEE Trans. Industrial Electronics,* vol. 50, no. 5, p.p. 962-981, Oct. 2003.

[2] X. Li and A. K. S. Bhat, "A Utility-Interfaced Phase-Modulated High-Frequency Isolated Dual LCL DC/AC Converter", *IEEE Trans. Industrial Electronics,* vol. 59, no. 2, p.p. 1008-1019, Feb. 2012.

[3] T. L. Vandoorn, B. Meersman, L. Degroote, B. Renders and L. Vandevelde, "A Control Strategy for Islanded Microgrids with DC-Link Voltage Control," *IEEE Trans. Power Delivery,* vol. 26, no. 2, p.p. 703-713, 2011.

[4] L. Xu and D. Chen, "Control and Operation of a DC Microgrid with Variable Generation and Energy Storage," *IEEE Trans. Power Delivery,* vol. 26, no. 4, p.p. 2513-2522, 2011.

[5] B. Yang, W. Li, Y. Zhao and X. He, "Design and Analysis of a Grid-Connected Photovoltaic Power System", *IEEE Trans. Power Electronics*, vol. 25, no. 4, pp. 992–1000, April 2010.

[6] H. M. Kojabadi, B. Yu, I. A. Gadoura, L. Chang and M. Ghribi, "A novel DSP-based current-controlled PWM strategy for single phase grid connected inverters," *IEEE Trans. Power Electronics* , vol. 21, no. 4, pp. 985–993, July 2006.

[7] Y. C. Chang and C. M. Liaw, "Establishment of a Switched-Reluctance Generator-Based Common Microgrid System," *IEEE Trans. Power Electronics* , vol. 26, no. 9, pp. 2512–2527, Sep. 2011.

[8] R. Wang, F. Wang, D. Boroyevich, R. Burgos, R. Lai, P. Ning and K. Rajashekara, "A High Power Density Single-Phase PWM rectifier with Active Ripple Energy Storage," *IEEE Trans. Power Electronics* , vol. 26, no. 5, pp. 1430–1443, May 2011.

[9] Y. K. Lo, "Dual hysteresis loops for a high-performance four-switch boost rectifier," *IEEE Trans. Industrial Electronics,* vol. 47, no. 5, p.p. 1174-1176, Oct. 2000.

[10] S. C. Yip, D. Y. Qiu, H. S. Chung, and S. Y. R. Hui, "A Novel Voltage Sensorless Control Technique for a Bidirectional AC/DC Converter", *IEEE Trans. on Power Electronics*, vol. 18, no. 6, pp. 1346-1355, Nov. 2003.

[11] H. C. Chen, C. C. Lin and J. Y. Liao, "Modified Single-Loop Current Sensorless Control for Single-Phase Boost-Type SMR with Distorted Input Voltage," *IEEE Trans. on Power Electronics*, vol. 26, no. 5, pp. 1322-1328, May 2011.